Received: 19 October 2023 | Accepted: 9 January 2024

DOI: 10.1111/ahe.13016

ORIGINAL ARTICLE

Anatomia Histologia Embryologia | WILEY

Computed tomographic study analysing functional biomechanics in the thoracolumbar spine of horses with and without spinal pathology

Natalie Baudisch[1] | Lukas Schneidewind[2] | Sophie Becke[2] | Max Keller[2] | Milena Overhoff[2] | Dennis Tettke[2] | Viola Gruben[3] | Fabienne Eichler[1] | Henning Jürgen Meyer[2] | Christoph Lischer[1] | Anna Ehrle[1]

[1]Equine Clinic, Veterinary Hospital Freie Universität Berlin, School of Veterinary Medicine, Berlin, Germany

[2]Chair Machinery System Design, Technische Universität Berlin, Berlin, Germany

[3]Faculty of Medical Engineering and Technomathematics, University of Applied Sciences Aachen, Jülich, Germany

Correspondence
Natalie Baudisch, Equine Clinic, Veterinary Hospital Freie Universität Berlin, School of Veterinary Medicine, Oertzenweg 19b, 14163 Berlin, Germany.
Email: n.baudisch@fu-berlin.de

Funding information
Akademie für Tiergesundheit; Verein zur Förderung der Forschung im Pferdesport e.V.; Elsa-Neumann-Scholarship; Gesellschaft zur Förderung der Forschung um das Pferd e.V.

Abstract

To better understand physiological and pathological movement patterns in the equine thoracolumbar spine, investigation of the biomechanics on a segmental level requires a constant moment. A constant moment along the spinal column means that the same torque acts on each vertebral segment, allowing the range of motion of different segments to be compared. The aims of this study were to investigate the range of motion of the equine thoracolumbar spine in horses with and without spinal pathology and to examine whether the pressure between the spinous processes depends on the direction of the applied moment. Thoracolumbar spine specimens (T8-L4) of 23 horses were mounted in a custom-made mechanical test rig to investigate spinal biomechanics during lateral bending, axial rotation, flexion and extension using computed tomographic imaging. Results were compared between horses with spondylosis, overriding spinous processes and specimens free of gross pathology. The interspinous space pressure was additionally determined using a foil sensor. The median lateral bending between T9 and L3 was 3.7°–4.1° (IQR 5.4°–8.0°). Maximum rotational movement with inconsistent coupled motion was observed at T9–T16 ($p < 0.05$). The dorsoventral range of motion was greatest in segments T9–T11 ($p < 0.05$). Spondylosis and overriding spinous processes restricted spinal mobility, depending on the severity of the condition. There was no significant difference in interspinous pressure during motion ($p = 0.54$). The biomechanical study confirmed that the range of motion of intervertebral joints depends on the anatomical position of the joint and the direction of the moment applied. Restricted mobility was evident in the presence of different grades of overriding spinous processes or spondylosis. A better understanding of equine spinal biomechanics in horses with spinal pathology facilitates individual rehabilitation.

KEYWORDS
biomechanics, horse, overriding spinous processes, spondylosis, thoracolumbar spine

1 | INTRODUCTION

Overriding spinous processes (ORSPs) are described as a common cause of thoracolumbar pain in horses but are also frequently identified in asymptomatic ridden horses (Cousty et al., 2010; de Graaf et al., 2015; Holmer et al., 2007; Ranner & Gerhards, 2002). Overriding or impinging spinous processes are defined as narrowing of the interspinous space to less than 4 mm, usually detected in the region between the 13th thoracic and the first lumbar vertebrae (Coomer et al., 2012; Cousty et al., 2010; Jacklin et al., 2014; Walmsley et al., 2002).

The aetiology of ORSPs is not fully understood. Whilst there is no evidence for radiographic changes in the area of the spinous processes (SPs) in Warmblood foals, ORSPs were detected in untrained Thoroughbred yearlings (Pressanto et al., 2023; Sinding & Berg, 2010). Fused SPs are found more frequently in older horses (Scilimati, Beccati, et al., 2023). A developmental or genetic component of the condition is the subject of current debate (Patterson Rosa et al., 2022; Pressanto et al., 2023). Alterations of the interspinous ligament structure and innervation have been associated with the pathogenesis of ORSPs (Ehrle et al., 2019). Additionally, Coomer et al. (2012) offered the theory that ORSPs may cause a compartment syndrome of the interspinous ligament (Coomer et al., 2012). To the best of the authors' knowledge, no study has further investigated this hypothesis so far.

When compared to ORSPs, spondylosis is less commonly diagnosed in the equine thoracolumbar spine (Jeffcott, 1980; Meehan et al., 2009). The condition describes large osteophytes covering the ventral or lateral aspect of the intervertebral discs between affected vertebrae and is most frequently identified at T11–T13 (Butler et al., 2017; Haussler, 1999; Meehan et al., 2009; Scilimati, Angeli, et al., 2023). Spondylosis is found more often in older horses (Scilimati, Angeli, et al., 2023).

The anatomy of the equine thoracolumbar spine allows three movement patterns, including lateral bending, axial rotation and flexion–extension (Panjabi & White III, 1980; Townsend et al., 1983). Previous studies investigating equine thoracolumbar spine kinematics demonstrated considerable variations in the range of motion (ROM) of different spinal segments, with the stiffness of the spine depending on the direction of the load applied (Faber et al., 2000, 2001a, 2001b; Jeffcott & Dalin, 1980; Schlacher et al., 2004; Townsend et al., 1983). A constant torque (independent of time) along the spinal column acting on each vertebral segment is required to compare the ROM of the different spinal segments. Torque is defined as the mathematical product of force and the lever arm (Latash & Zatsiorsky, 2016). To the best of the authors' knowledge, there is no advanced diagnostic imaging study investigating the three-dimensional ROM of the equine thoracolumbar spine with and without spinal pathology.

The targeted and successful rehabilitation of equine spinal conditions relies on the detailed understanding of the anatomical and biomechanical interrelation of spinal segments. The aim of this study was therefore to determine the ROM of the equine thoracolumbar spine with and without spinal pathology based on computed tomographic (CT) imaging and to investigate the forces acting on the interspinous ligaments. First, it was hypothesized that the ROM of each intervertebral joint depends on its respective spinal position. The second hypothesis was that pathological changes of the spine have an impact on the ROM of the affected segment. Third, the authors investigated whether the pressure between the SPs depends on the direction of the applied moment.

2 | MATERIALS AND METHODS

2.1 | Animals and samples

Equine thoracolumbar spine specimens of 23 skeletally mature horses (aged 2–29 years; median 17 years) euthanized for reasons unrelated to this study and without previous spinal pathology were included in the study. Informed owner consent for tissue retention was obtained, and the study was approved by the local research ethics committee (IVC1Schr-StN010/20). There were 13 geldings, 1 stallion and 9 mares. Breeds represented were one American Quarter horse, one Appaloosa, two Arabians, one Friesian, one Holsteiner, three Icelandic horses, one cold-blooded horse, two Ponies, one Trotter, nine warmbloods and one Welsh Cob.

Spines were excised between the seventh to eighth thoracic and the fourth to fifth lumbar vertebrae, with the ribs transected about 15 cm lateral to the spine at the level of the rib angle. The entire epaxial and hypaxial musculature, including the skin, were left intact. Specimens weighed 21–45 kg (median: 31 kg).

2.2 | Mechanical testing device

A custom-made aluminium/stainless-steel mechanical test rig consisting of a cranial and a caudal part was built to evaluate the spinal ROM within a Canon Large Bore scanner with a 32-slice detector (Figure 1). Thoracolumbar spine specimens were mounted in the rig with eight adjustable stainless-steel thorns (length 6.8 cm, diameter 1 cm) arranged in a clamping chuck. Thorns were tightened in a radial direction around the eighth/ninth thoracic and third/fourth lumbar vertebral bodies, respectively. The clamping chucks were attached to steel shafts to connect to the rig. Self-locking gearbox-translated handwheels on the cranial and caudal parts of the device were used to apply defined bending or torsional moments to the specimens. The applied torque was recorded using torque transducers (KKmoon; range 2–200 Nm, accuracy ±1%) that were positioned between the handwheel and shaft (Figure 2).

2.3 | Experimental procedure—biomechanical study

Initially, a CT scan of the entire specimen was acquired with the spine mounted in the mechanical testing device with no torque applied (neutral position). At this point, significant spinal pathology was identified and documented. Specimens were subsequently deflected

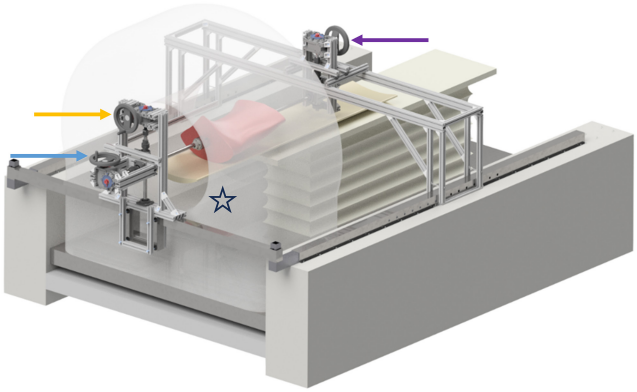

FIGURE 1 Mechanical test rig for computed tomographic imaging of an equine spine specimen (indicated in red) at deflection. Cranial part (left side of the image) with handwheels for lateral bending (yellow arrow) and rotation (blue arrow). Caudal part (right side of the image) with handwheel for lateral bending (purple arrow). For flexion and extension, specimens were positioned at 90° to the sagittal plane, and the handwheels for lateral bending were used to perform dorsoventral movement. Qalibra CT system equipped with a Canon Large Bore (32-slice detector) (transparent, marked with black star).

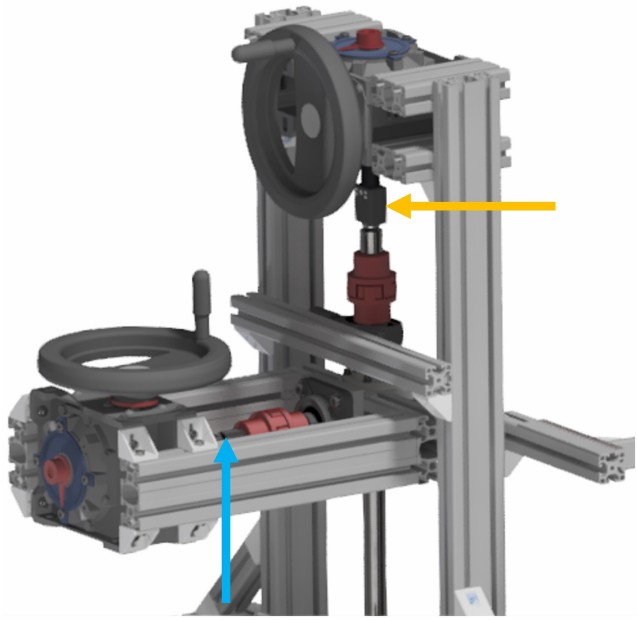

FIGURE 2 Close-up view of the cranial part of the test rig with a handwheel and torque transducer for lateral bending (yellow arrow) and axial rotation (blue arrow).

laterally (to the left and to the right side), left and right axial rotation and spinal flexion and extension were applied. A constant torque of 60 Nm was selected as it led to maximum spinal deflection in all directions. Due to the relaxation of the spine, the 60 Nm torque was constantly readjusted manually for 5 s before the self-locking state. CT imaging was performed following deflection and additionally in neutral position in between the different motion patterns (Figure 3).

Lateral bending was achieved using the handwheels on both sides of the specimens. Based on the principle of coupled motion, rotational movement was enabled. Rotational movement was applied via the cranial handwheel, with the caudal aspect of the specimen in a fixed position. For flexion and extension, specimens were positioned at 90° to the sagittal plane. Torque was applied as described for lateral movement, but with the rotational component in a fixed position. Specimens were supported by the CT couch during biomechanical testing to avoid an additional vertical bending moment caused by gravitational forces. As the applied movements were independent of forces resulting from gravitation, a constant moment was applied along the entire spine (Figure 4).

2.4 | CT image evaluation

The lateral ROM was assessed on coronal plane images. The angle deviation was determined based on the midline of the ninth thoracic and the third lumbar vertebral bodies (Figure 5).

The degree of axial rotation was measured in transverse plane images where the third lumbar vertebra served as a reference point (Figure 5). Initially, the rotation angle of each vertebra was determined. For analysis of the interspinous space rotation angle, the angle of the caudally located vertebra was subtracted from the adjacent cranial vertebra. The neutral position angle was subsequently subtracted from the left and right rotation angles.

The dorsoventral ROM was analysed on sagittal plane images (Figure 5). In line with previous reports, the dorsoventral ROM was measured as a distance (mm) not as an angle (Berner et al., 2012; Jeffcott & Dalin, 1980). For this purpose, a tangent line was inserted between the caudoventral extremity of a vertebral body and the most caudal aspect of the corresponding SPs (Berner et al., 2012). A line with the same length was applied to the flexed and extended spine images. A perpendicular line was further inserted between the most caudal aspect of the cranial SP and the adjacent caudal SP. The length of this line indicates the width of the interspinous space. To calculate a ratio, the width of the interspinous space during flexion and extension was divided by the width in neutral position.

All measurements were obtained by one blinded observer (N.B.). To calculate the inter-observer reliability, a subset of the measurements ($n = 41$) was additionally analysed by a second observer.

2.5 | Spinal pathology

ORSPs and spondylosis, as identified during CT image evaluation, were graded: For ORSPs, the description of Zimmerman et al. (2011) and for spondylosis, the grading system by Meehan et al. (2009) was used.

2.6 | Test procedure—pressure measurement

Following the biomechanical study, eight specimens without evidence of gross spinal pathology were randomly selected for

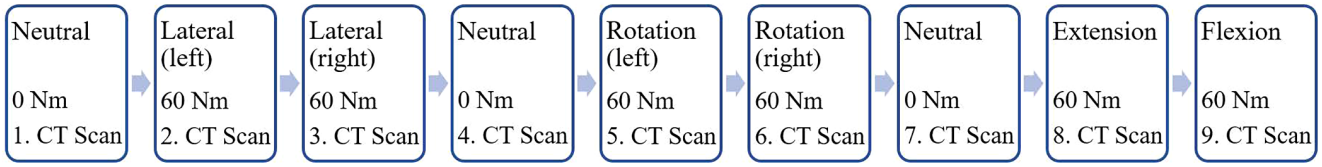

FIGURE 3 Experimental protocol for the biomechanical study.

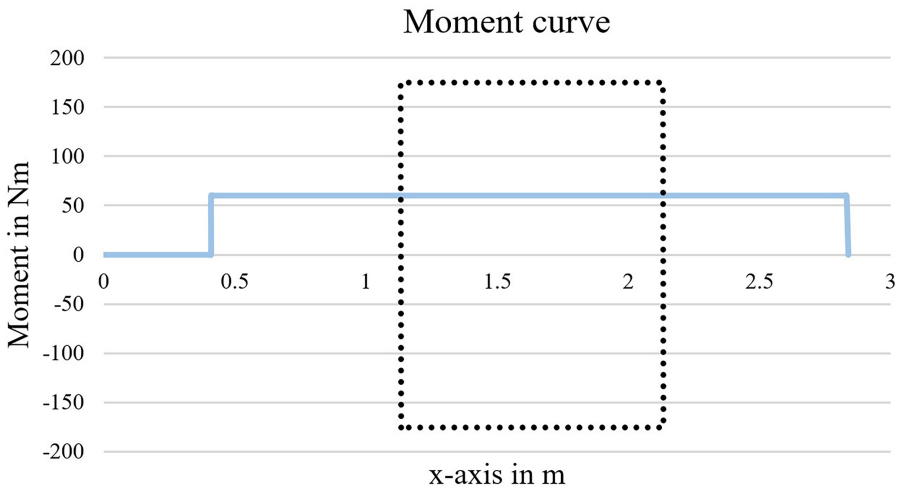

FIGURE 4 Moment curve for lateral bending. Blue line = torque moment; black dotted line = length of spine specimen in m (left = cranial, right = caudal). The applied torque of 60 Nm acts equally on all spinal segments.

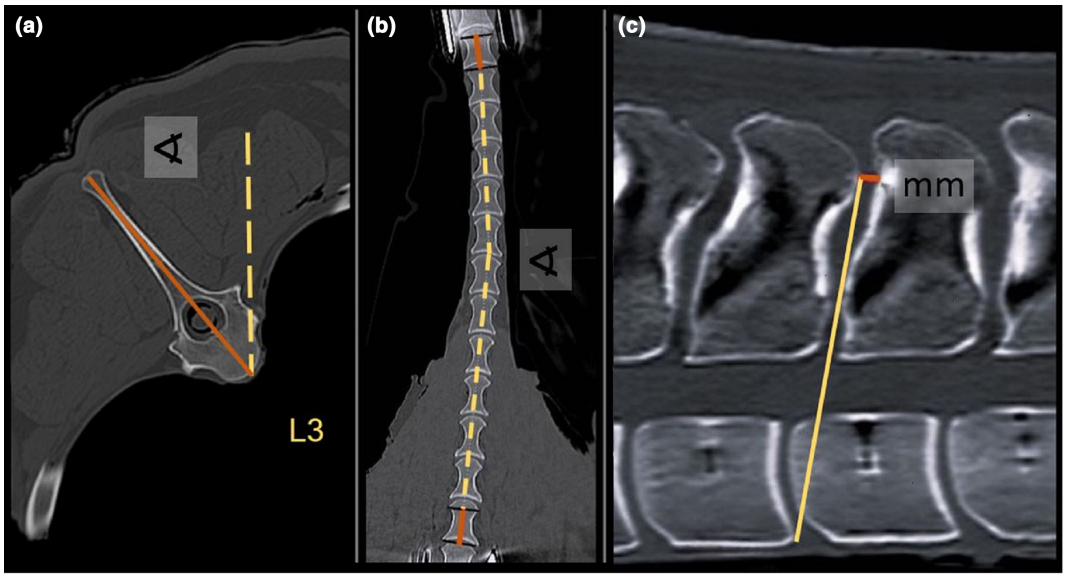

FIGURE 5 Computed tomographic images of the equine thoracic spine during different deflections. (a) Measurement of rotation at the level of the 10th thoracic vertebra: The third lumbar vertebra served as a reference point (yellow interrupted line), and the angle deviation to every vertebra was measured by inserting a sagittal line (orange line) between the dorsal aspect of the spinous process and the ventral aspect of the vertebral body. (b) Measurement of lateral bending: The angle deviation was determined based on the midline (orange lines) of the ninth thoracic and the third lumbar vertebral bodies. (c) Measurement of the interspinous distance: a line (yellow line) was inserted between the most caudal aspect of the cranial vertebral body and the most caudal aspect of the corresponding spinous process. A second line (orange line) was drawn perpendicular to the yellow line, starting at its dorsal aspect. This orange line was used to determine the width of the interspinous space (Berner et al., 2012). The percentage increase/narrowing in interspinous space width during dorsoventral movement (flexion/extension) was calculated as follows: 100 × (mm (dorsoventral) − mm (neutral))/mm (neutral) = %.

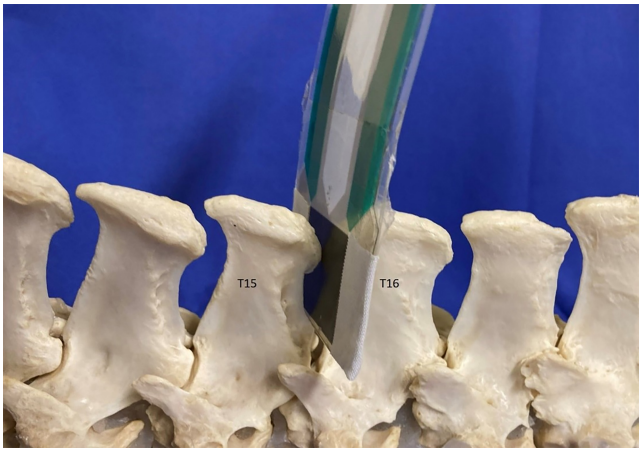

FIGURE 6 The position of the pressure transducer between the 15th and 16th thoracic vertebrae was demonstrated in a spine specimen without soft tissues attached.

pressure measurement within the interspinous space. A foil sensor (pressure mapping sensor; Tekscan, USA) with a resolution matrix of 27.9 × 27.9 mm and 1.936 sensels for pressure recording (pressure range 0–3448 kPa) was inserted in the interspinous space between the 15th and 16th thoracic vertebral SPs, where ORSPs commonly occur (Figure 6; Zimmerman et al., 2011).

The experimental protocol as described for the biomechanical study was subsequently repeated (Figure 3), but pressure measurements were obtained during the different motion patterns (neutral position, lateral bending, axial rotation, dorsoventral flexion and extension) instead of CT scans. The output of the pressure sensor foil refers to a colour scale with associated numerical intensity values ranging from 0 to 4000. To convert the numeric values into pressure values [mmHg], the calibration curve was implemented in a customized MatLab script (MatLab, R2020a). For pressure calculation, the sensor's signal noise was additionally subtracted from the measured values.

2.7 | Statistical analysis

Data were recorded in Excel (Version 2305; Microsoft Inc., Redmond, WA, USA) and statistically analysed using SPSS (IBM SPSS Statistics for Windows, Version 28.0. Armonk, NY, USA) and RStudio Team (2020, Version 20.0.0.0). Descriptive analysis was performed for the horses' age, the weight of the specimens, lateral bending and coupled motion. A non-parametric statistical test (Friedman test), a post-hoc test (Dunn-Bonferroni test) and the effect size (Cohen test) were used to determine statistically significant differences in the ROM between vertebrae during axial rotation and flexion–extension. The Friedman test was additionally used to identify statistically significant differences between the pressure measurements obtained during spinal deflection in different directions. p-Values < 0.05 were considered statistically significant. To document the intra- and inter-observer reliability for the ROM measurements and quantify the agreement of the pressure measurements, Lin's concordance correlation coefficient (CCC) was calculated.

3 | RESULTS

3.1 | Biomechanical study

The median distance between SPs, the 25th and 75th percentiles in neutral position and the ROM for lateral bending, axial rotation, flexion and extension for the 18 spinal specimens without gross pathologies are summarized in Table 1.

The median degree of lateral movement was 4.1° (IQR 5.4°) to the left and 3.7° (IQR 8.0°) to the right. The maximum degree of lateral movement was 24.5°.

There was a significant difference in the ROM between vertebrae during axial rotation to the left ($p < 0.001$, $n = 18$) and right side ($p < 0.001$, $n = 18$) (Figure 7). There was significantly ($p < 0.05$) more axial rotation between the thoracic (T9–T16) vertebrae than between the lumbar (L1–L3) vertebrae. Significantly more rotational movement was additionally identified when the individual spinal segments in the areas of T9–T15 and T17–L1 ($p < 0.05$) or T11–T14 and T16/T17 ($p < 0.05$) were compared. The effect size was largest between T12/T13 and L2/L3 for right rotation (effect size = 1.6) and between T12/T13 and L1/L2 for left rotation (effect size = 1.9). For right rotation, a median of 3.1° (interquartile range (IQR) = 2.1°) was obtained at the level T12/T13 and 0.3° (IQR = 0.9°) at L2/L3. For left rotation, a median of 3.7° (IQR = 1.8°) was calculated at T12/T13 and 0.4° at L1/L2 (IQR = 1.1°) (Table 1).

Coupled motion of axial rotation during lateral movement was documented, with 54% specimens rotating to the left and 46% to the right during left lateral movement. Lateral movement to the right resulted in rotation of the vertebrae to the right in 41% and to the left in 59% specimens. Vice versa, lateral bending during axial rotation was observed, with axial rotation to the right leading to lateral bending to the right in 55%, to the left in 36% and to no lateral bending in 9% of specimens. Axial rotation to the left was coupled with lateral bending to the left in 73% and to the right in 27% of specimens.

Dorsoventral movement analysis showed significant differences between spinal segments during flexion ($p < 0.001$, $n = 18$) and extension ($p < 0.001$, $n = 18$). There was significantly more movement between T9/T10 than between T12–T14, T15–T17 and T18–L3 during flexion. The largest effect size was identified when T9/T10 was compared with T15/T16 and L2/L3 (effect size = 1.3). The width of the T9/T10 interspinous space increased by a median of 48.5% (IQR 70%), 7.2% at T15/T16 (IQR 25%) and 9.2% at L2/L3 (IQR 11%) (Table 1). During extension, there was significantly more narrowing of the interspinous space between T9/T10 than between T12–T15 and T18–L3 ($p < 0.05$). Additionally, there was more narrowing of the interspinous space between T10/T11 when compared to the spaces T18-L3 ($p < 0.05$). The effect size was largest between T9/T10 and L1/L2 (effect size = 1.4). The median reduction in interspinous space

TABLE 1 Distance between the spinous processes in neutral position (Median=Md., 25%ile, 75%ile). Md. range of motion of the vertebrae (T9–L3) during lateral bending °, axial rotation °, flexion % and extension %.

Interspinous space	T9/T10	T10/T11	T11/T12	T12/T13	T13/T14	T14/T15	T15/T16	T16/T17	T17/T18	T18/L1	L1/L2	L2/L3
25%ile distance (mm)	4.0	4.7	6.2	6.2	4.7	3.7	4.5	5.8	4.8	6.8	6.9	7.9
Md. distance (mm)	5.1	6.4	7.7	8.7	7.6	6.7	6.9	6.6	7.3	9.4	11.0	9.8
75%ile distance (mm)	7.6	8.7	9.6	11.1	9.3	8.4	9.5	9.3	11.0	11.6	12.8	12
Left lateral bending (°)	4.1											
Right lateral bending (°)	3.7											
Left rotation (°)	2.1	2.6	3.4	3.7	3.0	2.8	2.0	1.2	1.2	0.5	0.4	0.4
Right rotation (°)	2.7	2.6	3.3	3.1	2.6	2.7	2.5	1.3	0.5	0.6	0.4	0.3
Flexion increase (%)	48.5	28.9	15.9	10.2	14.4	23.9	7.2	14.2	14.4	11.1	8.0	9.2
Extension narrowing (%)	−32.1	−29.4	−11.6	−6.8	−8.4	−10.4	−9.2	−6.4	−12.9	−4.1	−3.2	−4.1

width was −32.1% (IQR 32%) for T9/T10 and −3.2% (IQR 6%) for L1/L2 (Table 1).

The calculation of the intra-observer reliability identified a Lin's concordance correlation coefficient (CCC) of 0.963 (95% confidence interval 0.941–0.976). Lin's CCC for the inter-observer reliability was 0.676 (95% confidence interval 0.49–0.80).

3.2 | Spinal pathology

Gross pathological changes, including impinging dorsal spinous processes ($n=2$; Spines A and B) and spondylosis ($n=3$), were identified in five specimens. Biomechanical testing was performed as described (Figure 3), but results were excluded from the main study and are reported separately in the following paragraphs. Since no reliable method could be established to measure the lateral bending of individual spinal segments, the measurement was excluded from this part of the study. Results are presented in Tables 2 and 3.

3.3 | Overriding spinous processes

Lesions were graded based on the description of Zimmerman et al. (2011). Spine A showed a grade 5 lesion at site T13/T14 and a grade 4 lesion at T14/T15. Spine B had one grade 5 (T14/T15), two grade 2 lesions (T15/T16, T16/T17) and one grade 4 (T17/T18) lesion (Table 2). In spine A, rotation to the left was possible by 3.7° at the level of the grade 5 lesion and 4.3° at the grade 4 lesion. The interspinous space width did not increase at either site during flexion. Extension of the spine had no effect at the level of the grade 5 lesion but resulted in narrowing of the interspinous space by 6.7% (neutral 1.5 mm, extension 1.4 mm) at the level of the grade 4 lesion.

In spine B, rotation was possible by 2.4° (left rotation) – 3° (right rotation) for the grade 5 lesion, 2.2°–2.6° for grade 2 at T15/T16, 0°–1.7° for grade 2 at T16/T17 and 1.6°–1.7° for the grade 4 lesion. Flexion resulted in an increase of the interspinous space width of 1.9 mm at the level of the grade 5 lesion (neutral 1.4 mm, increase 135.7%), 0.4 mm for the grade 2 lesion at T15/T16 (neutral 3.2 mm, increase 12.5%), 1.8 mm for the grade 2 lesion at T16/T17 (neutral 2.6 mm, increase 69.2%) and 1.1 mm for the grade 4 lesion (neutral 2.5 mm, increase 44%). Extension led to a narrowing of the interspinous space by 0.2 mm for grade 5 (decrease 14.3%), 0.9 mm for grade 2 at T15/T16 (decrease 28.1%), 1.4 mm for grade 2 at T16/T17 (decrease 53.8%) and 1.2 mm for the grade 4 lesion (decrease 48%).

3.4 | Spondylosis

Spondylosis (T9–T16) was graded using the system described by Meehan et al. (2009). Grade 5 spondylosis (complete bridging of intervertebral space) was detected at eight sites (once at sites T12/T13, T15/T16 and twice at sites T10/T11, T11/T12 and T13/T14) and

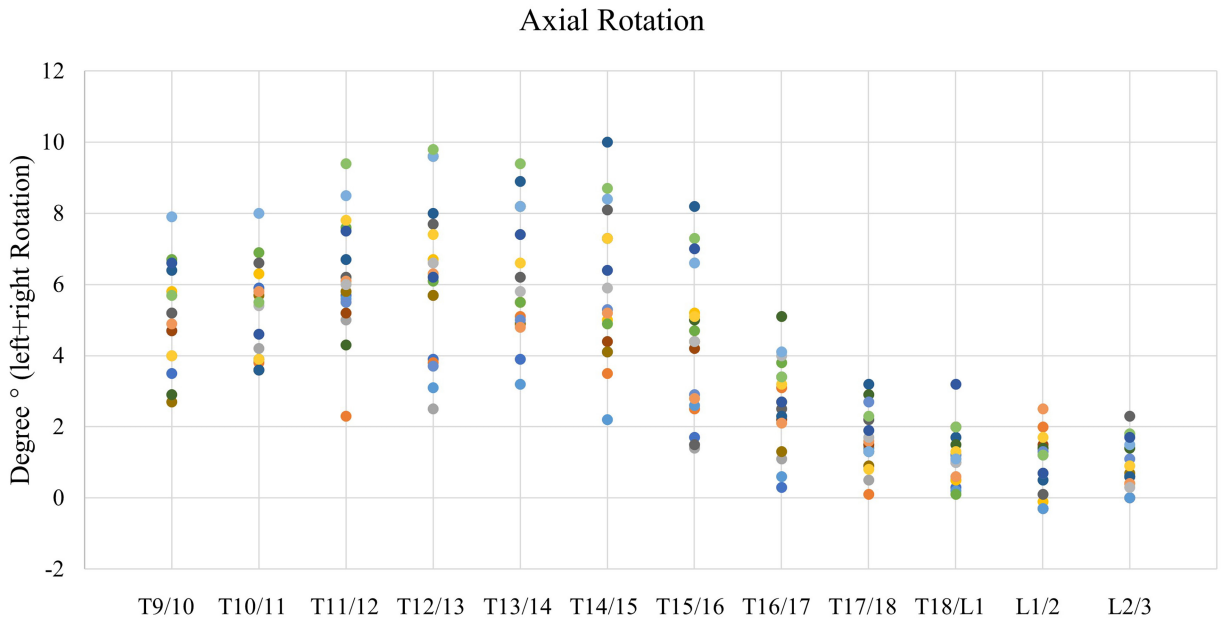

FIGURE 7 Degree of axial rotation of each spinal segment. *x*-axis, spinal segments T9–L3; *y*-axis, degree of axial rotation (sum of left and right rotation). Each colour represents a spine specimen.

grade 4 spondylosis at six sites (once at T9/T10, T11/T12, T13/T14, T14/T15 and twice at T12/T13). Grade 1 ($n=3$) and grade 3 ($n=1$) lesions were also detected, but due to the small quantity, they are not analysed in detail here. The ROM of the spinal segments in the area of interest is shown in Table 3. The median ROM for rotation, flexion and extension was calculated. Right rotation was possible by a median of 0.85° (IQR 1.53°) and left rotation by a median of 0.35° (IQR 0.75°) in grade 5 spondylosis. Sites with grade 4 spondylosis showed right rotation by a median of 2.4° (IQR 3.5°) and left rotation by a median of 3.4° (IQR 1.9°). The median increase in interspinous space width during flexion with grade 5 spondylosis was 0.0% (IQR 1.8%) and 13.1% (IQR 15.6%) with grade 4. The median narrowing of the interspinous space during extension with grade 5 spondylosis was −3.5% (IQR 6.3%), and with grade 4 −6.2% (IQR 18.9%).

3.5 | Pressure measurement

Following noise subtraction, the median pressure between the T15/T16 SPs ranged from 580.7 to 595.3 mmHg (Figure 8). No significant difference in pressure during the different deflections was identified ($p=0.54$, $n=8$). To evaluate the reproducibility, Lin's CCC was calculated with a result of 0.80 (95% confidence interval = 0.60–0.91).

4 | DISCUSSION

The biomechanical study of the equine thoracolumbar spine confirmed significant variations in the ROM between the intervertebral joints of adjacent spinal segments (first hypothesis). Restricted mobility was evident in the presence of different grades of ORSPs or spondylosis (second hypothesis). An influence of the direction of the applied torque on the pressure between SPs was not identified (third hypothesis).

The main focus during the experimental setup was to subject all vertebrae to the same torque in order to compare the mobility of individual vertebrae. The design of the custom-made test rig used facilitates the application of a torque that impacts each individual vertebra with constant intensity. The torque application was implemented by a manual and translated torque applications on the cranial and caudal aspects of the spine. Townsend et al. (1983) clamped the spine permanently on one side and deflected it with force on the other side, which results in a maximum bending moment on the clamped side and no bending moment on the deflected side (Townsend et al., 1983). If the spine is fixed on both sides and loaded centrally, as performed by Jeffcott and Dalin (1980), the middle of the spine is exposed to a local maximum (Jeffcott & Dalin, 1980). To account for tissue relaxation, measurements were standardized by readjusting the applied torque 5 s prior to CT image acquisition in the current study. It is unclear how long the force was applied to the spines in other studies before images or measurements were obtained (Denoix, 1999; Jeffcott & Dalin, 1980; Townsend et al., 1983). Variable forces applied as well as potential tissue relaxation might explain different observations in previous studies (Denoix, 1999; Jeffcott & Dalin, 1980; Townsend et al., 1983).

For lateral bending, the overall mobility of the spine was determined. Due to the small individual ROM, the development of a reliable method for calculation of the lateral mobility for individual vertebrae proved to be challenging. Whilst Jeffcott and Dalin (1980) describe that lateral motion only occurs cranial to the 13th thoracic vertebra, Denoix (1999) reported lateral motion of up to 30° between T14 and L1. By applying 60 Nm in the current study, a

TABLE 2 Range of motion of spine specimens (A and B) with overriding spinous processes in rotation, flexion and extension. Lateral bending is not represented here as it was measured over the entire spine and not for individual segments. Right rotation in spine A was not measured due to technical difficulties.

Interspinous space	T13/T14	T14/T15		T15/T16	T16/T17	T17/T18
Spine A	Grade 5	Grade 4				
Spine B			Grade 5	Grade 2	Grade 2	Grade 4
Neutral distance (mm)	1.0	1.5	1.4	3.2	2.6	2.5
Left rotation (°)	3.7	4.3	2.4	2.6	0.0	1.7
Right rotation (°)	–	–	3.0	2.2	1.7	1.6
Flexion distance (mm)	1.0	1.5	3.3	3.6	4.4	3.6
Flexion increase (%)	0.0	0.0	135.7	12.5	69.2	44.0
Extension distance (mm)	1.0	1.4	1.2	2.3	1.2	1.3
Extension narrowing (%)	0.0	−6.7	−14.3	−28.1	−53.8	−48.0

TABLE 3 Range of motion of spine specimens (C, D and E) with spondylosis in rotation, flexion and extension. Bold characters = Grade 5.

Interspinous space	T9/T10	T10/T11	T11/T12	T12/T13	T13/T14	T14/T15	T15/T16
Spine C	Grade 4	Grade 5	Grade 5	Grade 5	Grade 5	Grade 4	Grade 5
Spine D	Grade 1	Grade 5	Grade 5	Grade 4	Grade 5	Grade 1	
Spine E		Grade 3	Grade 4	Grade 4	Grade 4	Grade 1	
Left rotation (°)	C = 1.8	**C = 1.9**	**C = 0.8**	**C = 0.0**	**C = 0.2**	C = 5.6	**C = 0.8**
	D = 4.0	**D = 0.0**	**D = 0.0**	D = 3.4	**D = 0.6**	D = 2.8	D = 2.8
	E = 3.3	E = 2.6	E = 3.4	E = 4.4	E = 3.2	E = 4.6	E = 2.5
Right rotation (°)	C = 1.3	**C = 0.0**	**C = 1.0**	**C = 0.5**	**C = 1.8**	C = 0.3	**C = 1.2**
	D = 3.0	**D = 1.7**	**D = 0.6**	D = 0.8	**D = 2.0**	D = 2.5	D = 0.4
	E = 3.0	E = 3.1	E = 4.8	E = 3.5	E = 4.0	E = 3.9	E = 3.6
Flexion increase (%)	C = 17.9	**C = 0.0**	**C = 1.3**	**C = 5.5**	**C = 0.0**	C = 3.6	**C = 0.0**
	D = 7.0	**D = 0.0**	**D = 0.0**	D = 17.0	**D = 2.0**	D = 38.5	D = 23.3
	E = 205.3	E = 6.2	E = 0.0	E = 19.3	E = 9.1	E = 0.0	E = 3.8
Extension narrowing (%)	C = −10.5	**C = −6.5**	**C = −2.6**	**C = 0.0**	**C = 0.0**	C = −14.5	**C = −4.3**
	D = −10.1	**D = 0.0**	**D = −5.5**	D = 0.0	**D = −7.1**	D = −17.3	D = −9.3
	E = −36.8	E = −46.2	E = −31.9	E = 0.0	E = −1.8	E = −10.7	E = −13.5

maximum lateral ROM of 24.5° was evident between T9 and L3. Denoix (1999) dissected the axial skeleton and replaced the attached muscles with straps. The straps were stretched to mobilize the spine in a dorsoventral and horizontal plane. The amount of force applied by Denoix is, however, uncertain, as a range between 50 and 400 N was described (Denoix, 1999). By applying a torque of 60 Nm in the present study, a maximum lateral ROM of 24.5° was identified over the spinal segments between T9 and L3 (median: left bending 4.1°; right bending 3.7°). The high variation in lateral mobility between specimens seen in the present study might be related to the horses' age, breed or positioning of the specimens. In line with previous biomechanical studies more axial rotation was observed in the cranial thoracic region (T9–T16) when compared to the caudal thoracic and lumbar segments (T17 – L3) (Denoix, 1999; Townsend et al., 1983).

Considering the dorsoventral ROM, Denoix (1999) found the greatest ROM between T14 and T18 (Denoix, 1999). Townsend et al. (1983) did not describe significant differences in the area of T2 – L6. In the present study, the dorsoventral ROM between T9 and T10 was significantly higher when compared to most segments further caudally. However, interspinous space T14/T15 allowed most flexion after T9–T11, which is consistent with the results of Denoix (1999). Similar to Denoix, Jeffcott and Dalin's findings, least dorsoventral mobility was present in the lumbar region (L1–L3) in the current study (Denoix, 1999; Jeffcott & Dalin, 1980). During extension, the greatest narrowing of the interspinous space occurred in the cranial spinal segments (T9–T11). Also, in the study by Berner et al. (2012), the greatest percentage narrowing appears to be in the T9–T11 region. In this study, radiographic examinations of the thoracic spine of horses were performed with the head in either neutral, high or low position. This resulted in flexion or extension of the thoracolumbar spine, and the narrowing or widening of the interspinous spaces was measured (Berner et al., 2012). Denoix (1999), on the other hand, found that the segments T14–T18 have a slightly greater ROM during extension

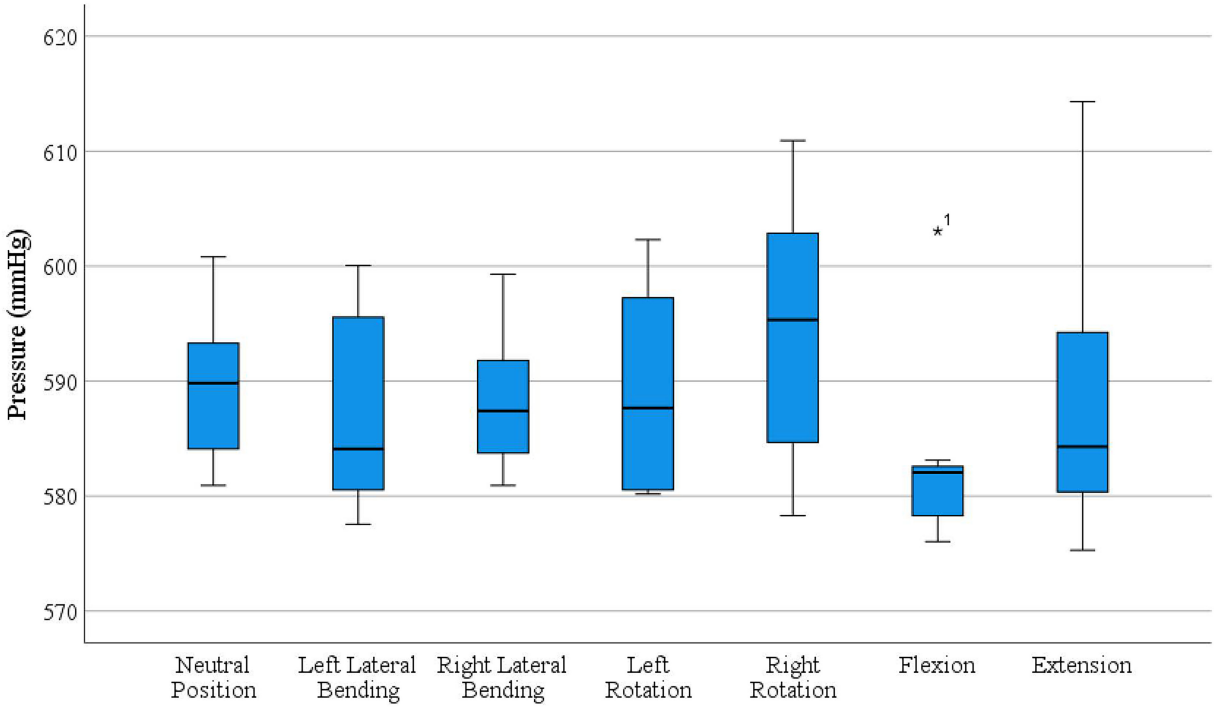

FIGURE 8 Boxplot representing pressure measured in the interspinous space between T15 and T16 with the spine deflected in different directions (lateral bending, axial rotation, flexion and extension). Black lines represent the median. Whiskers represent values outside the interquartile range. Extreme values are indicated by asterisks (*). There was no significant difference in pressure during the different deflections in thoracolumbar specimens without spinal pathology.

than the T9–T14 (Denoix, 1999). Our results suggest that there is no correlation between the location of ORSPs, mostly between T13 and L1, and the area with the greatest percentage narrowing during extension (T9–11) (Coomer et al., 2012; Cousty et al., 2010; Jacklin et al., 2014; Walmsley et al., 2002).

The principle of coupled motion with a consistent association of lateral bending with axial rotation is described for the equine thoracolumbar spine (Denoix, 1999; Townsend et al., 1983). The spine is supposed to bend laterally in the direction opposite to the rotation (e.g. left lateral bending during rotation to the right). The results of this study do not consistently support this observation. Whilst vertebrae rotated during lateral bending and vice versa, motion did not always occur in opposite directions. Coupled motion has also been described in humans, where the thoracic spine rotates to the same side and the lumbar spine to the opposite side during lateral bending (Fujimori et al., 2014; Liebsch et al., 2018; Narimani & Arjmand, 2018). As the results of human studies cannot be directly compared with those of equine species and spinal specimens without muscle tone were used in our study, additional research might be required to further elucidate coupled motion at the level of different spinal segments.

The investigation of the influence of pathological changes on spinal biomechanics confirmed restricted spinal mobility in the presence of ORSPs or spondylosis. Grade 5 ORSPs resulted in complete prevention of flexion in one spine and an increase in interspinous space width by 136% in the other. Whilst 136% appears to be a lot, the distance in mm by which the interspinous space increased is still very small. In neutral position, this interspinous space was 1.4 mm wide, with an increase to 3.3 mm during flexion. Compared to the interspinous space of a spine without pathology, maximum flexion in a grade 5 ORSPs lesion did not reach the median width of a normal interspinous space in neutral position. During extension, the distance between SPs decreased by a maximum of 0.2 mm with grade 5 ORSPs and by 0.1–1.2 mm in grade 4 lesions, indicating a partial ROM reduction. Rotation was least limited at ORSP sites.

Grade 5 spondylosis resulted in a complete loss of the ability to flex, with very little remaining extension and rotation. The small amount of mobility detected during extension and rotation may be associated with residual mobility or measurement irregularities. Grade 4 spondylosis primarily led to restricted flexion, which is most likely related to the interference of new bone formation in adjacent vertebrae.

Ehrle et al. (2019) identified different grades of fibrocartilaginous metaplasia in the interspinous ligament of horses with ORSPs (Ehrle et al., 2019). This observation would explain the results of the current study, where the intervertebral ROM decreased with increasing ORSPs grade but showed high variability between different specimens (e.g. interspinous space width increase during flexion in grade 5 lesions: 0% in spine A vs. 136% in spine B). The extent to which the interspinous ligaments have already undergone fibrocartilaginous metaplasia was, however, not assessed in this study.

Fibrocartilaginous metaplasia may be a result of compressive forces acting on the interspinous ligament as it is situated between the SPs (Ehrle et al., 2019). Initially, pressure measurement was

attempted using a needle tip pressure sensor (Gaeltec, Isle of Skye, Scotland) inserted centrally between the axial layers of the interspinous ligament (Ehrle et al., 2017). As measurements were not accurate enough with this sensor at this specific anatomical site, a foil sensor was used instead. The pressure values recorded were homogeneous amongst the different deflections as well as the different specimens analysed, indicating a constant pressure during variable movement patterns in the absence of ORSPs. Adjacent SPs did not touch each other during any movement pattern at maximum deflection in the current study, which likely explains why no pressure differences were detected. Whether there is interference of adjacent SPs leading to the development of ORSPs in some horses or excessive tension on the interspinous ligaments during flexion is responsible for the development of fibrocartilaginous metaplasia and subsequent ORSPs is yet to be determined (Benjamin & Ralphs, 1998).

The limitations of the study are the ex vivo character with limited number of specimens included for the analysis of pathological conditions. The influence of muscle activity on equine spinal biomechanics was not accounted for in the current study. Additionally, there might be an influence of compensatory movement in horses with spinal pathology. Comparison with in vivo studies is hampered by the varying experimental setups, including the investigation of the spinal ROM at different gaits. Future research may investigate the tensile forces acting on the interspinous ligament in motion. Additionally, further studies may elucidate the characteristics of coupled motion on a segmental level and reveal more detail about the influence of pathological conditions on the biomechanics of the equine thoracolumbar spine.

5 | CONCLUSION

The biomechanical study of the equine thoracolumbar spine confirmed that the ROM of the intervertebral joints depends on the anatomical position of the joint and the direction of the moment applied. The pattern of coupled motion was inconsistent and requires further investigation. Spondylosis and ORSPs limit the thoracolumbar ROM. An increase in interspinous pressure that could lead to a compartment syndrome during maximal extension was not documented in the current study. Further research investigating the tensile forces acting on the interspinous ligaments would be of great interest.

ACKNOWLEDGEMENTS

The authors gratefully acknowledge the support of Dorothea Treß in contributing to the execution of the study. We would further like to thank the team of post-mortem technicians of the Institute of Veterinary Pathology of the Freie Universität Berlin for their technical assistance. Additionally, we would like to thank the Verein zur Förderung der Forschung im Pferdesport e.V., Gesellschaft zur Förderung der Forschung um das Pferd e.V., Elsa-Neumann-Scholarship and Akademie für Tiergesundheit for their financial support. Open Access funding enabled and organized by Projekt DEAL.

CONFLICT OF INTEREST STATEMENT

None of the authors has any financial or personal relationships that could inappropriately influence or bias the content of the paper.

DATA AVAILABILITY STATEMENT

The data that support the findings of this study are available from the corresponding author upon reasonable request.

REFERENCES

Benjamin, M., & Ralphs, J. R. (1998). Fibrocartilage in tendons and ligaments – an adaptation to compressive load. *Journal of Anatomy*, *193*, 481–494. https://doi.org/10.1046/j.1469-7580.1998.19340481.x

Berner, D., Winter, K., Brehm, W., & Gerlach, K. (2012). Influence of head and neck position on radiographic measurement of intervertebral distances between thoracic dorsal spinous processes in clinically sound horses. *Equine Veterinary Journal*, *44*, 21–26. https://doi.org/10.1111/j.2042-3306.2012.00678.x

Butler, J. A., Colles, C. M., Dyson, S. J., Kold, S. E., & Poulos, P. W. (2017). *Clinical radiology of the horse* (4th ed.). John Wiley & Sons, Incorporated.

Coomer, R. P., McKane, S. A., Smith, N., & Vandeweerd, J. M. (2012). A controlled study evaluating a novel surgical treatment for kissing spines in standing sedated horses. *Veterinary Surgery*, *41*(7), 890–897. https://doi.org/10.1111/j.1532-950X.2012.01013.x

Cousty, M., Retureau, C., Tricaud, C., Geffroy, O., & Caure, S. (2010). Location of radiological lesions of the thoracolumbar column in French trotters with and without signs of back pain. *The Veterinary Record*, *166*(2), 41–45. https://doi.org/10.1136/vr.c70

de Graaf, K., Enzerink, E., van Oijen, P., Smeenk, A., & Dik, K. J. (2015). The radiographic frequency of impingement of the dorsal spinous processes at purchase examination and its clinical significance in 220 warmblood sporthorse. *Pferdeheilkunde*, *31*(5), 461–468. https://doi.org/10.21836/PEM20150505

Denoix, J. M. (1999). Spinal biomechanics and functional anatomy. *The Veterinary Clinics of North America: Equine Practice*, *15*(1), 27–60. https://doi.org/10.1016/s0749-0739(17)30162-1

Ehrle, A., Ressel, L., Ricci, E., Merle, R., & Singer, E. R. (2019). Histological examination of the interspinous ligament in horses with overriding spinous processes. *Veterinary Journal*, *244*, 69–74. https://doi.org/10.1016/j.tvjl.2018.12.012

Ehrle, A., Ressel, L., Ricci, E., & Singer, E. R. (2017). Structure and innervation of the equine supraspinous and interspinous ligaments. *Anatomia, Histologia, Embryologia*, *46*(3), 223–231. https://doi.org/10.1111/ahe.12261

Faber, M., Johnston, C., Schamhardt, H., van Weeren, R., Roepstorff, L., & Barneveld, A. (2001a). Basic three-dimensional kinematics of the vertebral column of horses trotting on a treadmill. *American Journal of Veterinary Research*, *62*(5), 757–764. https://doi.org/10.2460/ajvr.2001.62.757

Faber, M., Johnston, C., Schamhardt, H. C., van Weeren, P. R., Roepstorff, L., & Barneveld, A. (2001b). Three-dimensional kinematics of the equine spine during canter. *Equine Veterinary Journal*, *33*(S33), 145–149. https://doi.org/10.1111/j.2042-3306.2001.tb05378.x

Faber, M., Schamhardt, H., van Weeren, R., Johnston, C., Roepstorff, L., & Barneveld, A. (2000). Basic three-dimensional kinematics of the vertebral column of horses walking on a treadmill. *American Journal of Veterinary Research*, *61*(4), 399–406. https://doi.org/10.2460/ajvr.2000.61.399

Fujimori, T., Iwasaki, M., Nagamoto, Y., Matsuo, Y., Ishii, T., Sugiura, T., Kashii, M., Murase, T., Sugamoto, K., & Yoshikawa, H. (2014). Kinematics of the thoracic spine in trunk lateral bending: In vivo

three-dimensional analysis. *The Spine Journal*, *14*(9), 1991–1999. https://doi.org/10.1016/j.spinee.2013.11.054

Haussler, K. K. (1999). Anatomy of the thoracolumbar vertebral region. *Veterinary Clinics of North America: Equine Practice*, *15*(1), 13–26. https://doi.org/10.1016/S0749-0739(17)30161-X

Holmer, M., Wollanke, B., & Stadtbäumer, G. (2007). X-ray alterations on spinal processes of 295 warmblood horses without clinical findings. *Pferdeheilkunde*, *23*(5), 507–511.

Jacklin, B. D., Minshall, G. J., & Wright, I. M. (2014). A new technique for subtotal (cranial wedge) ostectomy in the treatment of impinging/overriding spinous processes: Description of technique and outcome of 25 cases. *Equine Veterinary Journal*, *46*(3), 339–344. https://doi.org/10.1111/evj.12215

Jeffcott, L. B. (1980). Disorders of the thoracolumbar spine of the horse – A survey of 443 cases. *Equine Veterinary Journal*, *12*(4), 197–210. https://doi.org/10.1111/j.2042-3306.1980.tb03427.x

Jeffcott, L. B., & Dalin, G. (1980). Natural rigidity of the horse's backbone. *Equine Veterinary Journal*, *12*(3), 101–108. https://doi.org/10.1111/j.2042-3306.1980.tb03393.x

Latash, M. L., & Zatsiorsky, V. M. (2016). 1 – Joint torque. In M. L. Latash & V. M. Zatsiorsky (Eds.), *Biomechanics and motor control* (pp. 3–24). Academic Press.

Liebsch, C., Graf, N., & Wilke, H.-J. (2018). The effect of follower load on the intersegmental coupled motion characteristics of the human thoracic spine: An in vitro study using entire rib cage specimens. *Journal of Biomechanics*, *78*, 36–44. https://doi.org/10.1016/j.jbiomech.2018.06.025

Meehan, L., Dyson, S., & Murray, R. (2009). Radiographic and scintigraphic evaluation of spondylosis in the equine thoracolumbar spine: A retrospective study. *Equine Veterinary Journal*, *41*(8), 800–807. https://doi.org/10.2746/042516409x436592

Narimani, M., & Arjmand, N. (2018). Three-dimensional primary and coupled range of motions and movement coordination of the pelvis, lumbar and thoracic spine in standing posture using inertial tracking device. *Journal of Biomechanics*, *69*, 169–174. https://doi.org/10.1016/j.jbiomech.2018.01.017

Panjabi, M. M., & White, A. A., III. (1980). Basic biomechanics of the spine. *Neurosurgery*, *7*(1), 76–93. https://doi.org/10.1227/00006123-198007000-00014

Patterson Rosa, L., Whitaker, B., Allen, K., Peters, D., Buchanan, B., McClure, S., Honnas, C., Buchanan, C., Martin, K., Lundquist, E., Vierra, M., Foster, G., Brooks, S. A., & Lafayette, C. (2022). Genomic loci associated with performance limiting equine overriding spinous processes (kissing spines). *Research in Veterinary Science*, *150*, 65–71. https://doi.org/10.1016/j.rvsc.2022.06.015

Pressanto, M. C., Pepe, M., Coomer, R. P., Pilati, N., & Beccati, F. (2023). Radiographic abnormalities of the thoracolumbar spinous processes do not differ between yearling and trained thoroughbred horses without perceived back pain. *Journal of the American Veterinary Medical Association*, *261*(6), 844–851. https://doi.org/10.2460/javma.22.09.0419

Ranner, W., & Gerhards, H. (2002). The occurrence of backproblems in horses in South Germany – With special reference to the 'kissing spine-syndrome'. *Pferdeheilkunde*, *18*(1), 21–33. https://doi.org/10.21836/PEM20020103

Schlacher, C., Peham, C., Licka, T., & Schobesberger, H. (2004). Determination of the stiffness of the equine spine. *Equine Veterinary Journal*, *36*(8), 699–702. https://doi.org/10.2746/0425164044848055

Scilimati, N., Angeli, G., Di Meo, A., Dall'Aglio, C., Pepe, M., & Beccati, F. (2023). Post-mortem computed tomographic features of the most caudal lumbar vertebrae, anatomical variations and acquired osseous pathological changes, in a mixed population of horses. *Animals*, *13*(4), 743. https://doi.org/10.3390/ani13040743

Scilimati, N., Beccati, F., Dall'Aglio, C., Di Meo, A., & Pepe, M. (2023). Age and sex correlate with bony changes and anatomic variations of the lumbosacroiliac region of the vertebral column in a mixed population of horses. *Journal of the American Veterinary Medical Association*, *261*(2), 258–265. https://doi.org/10.2460/javma.22.07.0293

Sinding, M. F., & Berg, L. C. (2010). Distances between thoracic spinous processes in warmblood foals: A radiographic study. *Equine Veterinary Journal*, *42*(6), 500–503. https://doi.org/10.1111/j.2042-3306.2010.00113.x

Townsend, H. G., Leach, D. H., & Fretz, P. B. (1983). Kinematics of the equine thoracolumbar spine. *Equine Veterinary Journal*, *15*(2), 117–122. https://doi.org/10.1111/j.2042-3306.1983.tb01732.x

Walmsley, J. P., Pettersson, H., Winberg, F., & McEvoy, F. (2002). Impingement of the dorsal spinous processes in two hundred and fifteen horses: Case selection, surgical technique and results. *Equine Veterinary Journal*, *34*(1), 23–28.

Zimmerman, M., Dyson, S., & Murray, R. (2011). Comparison of radiographic and scintigraphic findings of the spinous processes in the equine thoracolumbar region. *Veterinary Radiology & Ultrasound*, *52*(6), 661–671. https://doi.org/10.1111/j.1740-8261.2011.01845.x

How to cite this article: Baudisch, N., Schneidewind, L., Becke, S., Keller, M., Overhoff, M., Tettke, D., Gruben, V., Eichler, F., Meyer, H. J., Lischer, C., & Ehrle, A. (2024). Computed tomographic study analysing functional biomechanics in the thoracolumbar spine of horses with and without spinal pathology. *Anatomia, Histologia, Embryologia*, *53*, e13016. https://doi.org/10.1111/ahe.13016